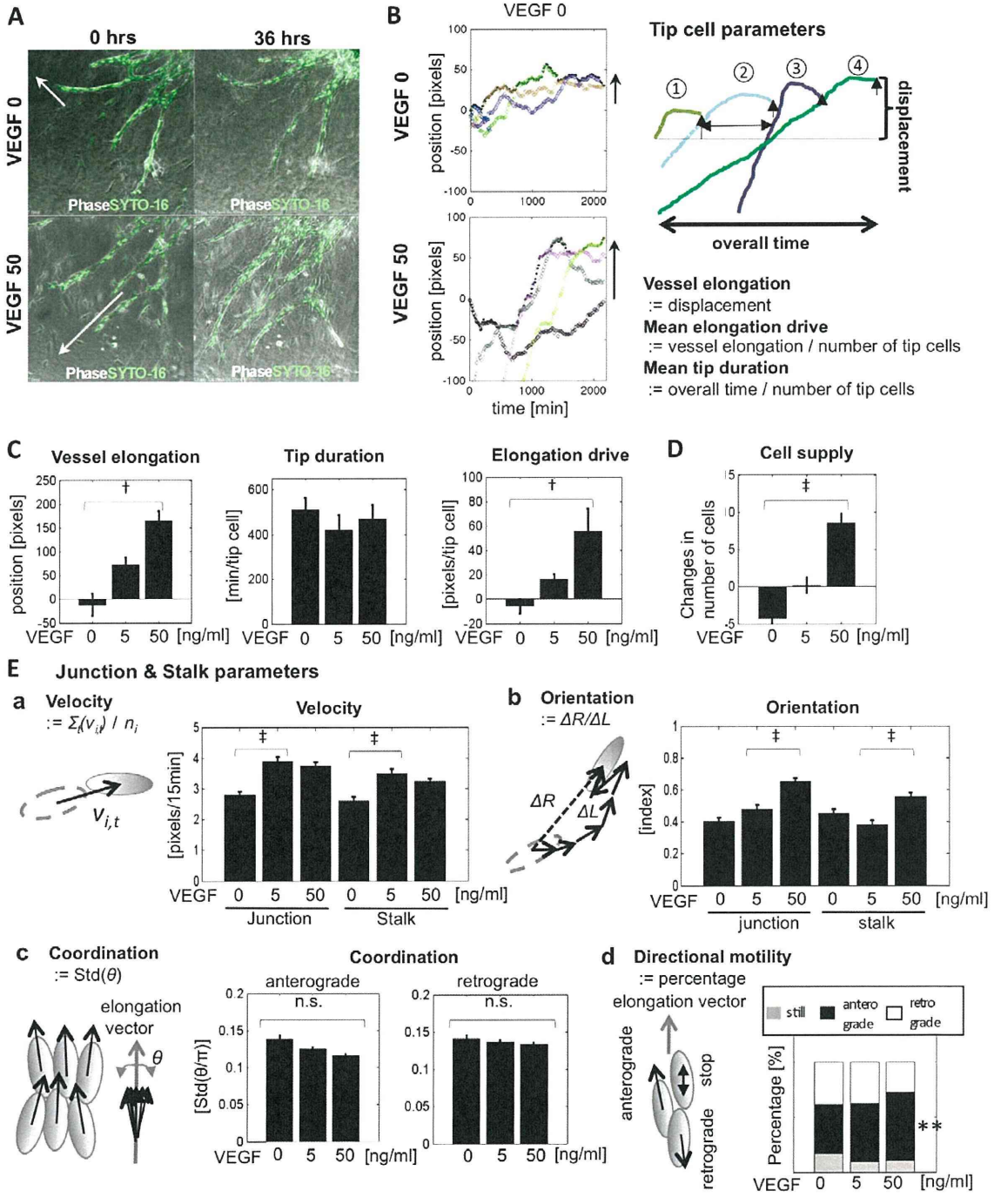

Fig. 5. Quantification of EC behaviors driving VEGF-induced angiogenic morphogenesis. (**A**) Time-lapse imaging in the murine aortic ring assay with or without VEGF. Arrows show the elongation vectors of selected branches (see also Movie 6 in the supplementary material). (**B**,**C**) Trajectory analysis (B, left panel) and parameters related to tip cells (B, right panel; C). (**D**) Cell supply (defined as changes in the number of cells in a branch). (**E**) Parameters at junctions and stalks. (a) EC velocity. (b) Orientation. (c) Coordination. (d) Directional motility (** significantly different from VEGF 0 ng/ml). Data are presented as mean±s.e.m. $^{**}P<0.01$, $^{\dagger}P<0.001$, $^{\ddagger}P<0.0001$.

presence of VEGF, ECs exhibited higher velocity and orientation at junctions and stalks (Fig. 5E-a,E-b). Coordination tended to be improved ($P=0.051$, for VEGF 0 ng/ml versus 50 ng/ml, Fig. 5E-c). At stalks, there was a higher proportion of ECs showing anterograde movement (Fig. 5E-d). Taken together, these data suggest that VEGF enhanced directed migration of ECs in the elongating direction at junctions and stalks. Parameters presented here are summarized in Fig. S6A in the supplementary material.

Dll4-Notch signaling pathway in collective EC movement driving angiogenic morphogenesis

To further define the molecular machinery involved in collective EC movements during angiogenesis, we interrupted Dll4-Notch signaling, which is crucial for tip cell regulation and proper angiogenesis (Hellstrom et al., 2007; Suchting et al., 2007). Consistent with previous findings (Claxton and Fruttiger, 2004; Hellstrom et al., 2007; Hofmann and Luisa Iruela-Arispe, 2007), Dll4 was expressed in ECs at the tip and, to a lesser extent, at stalks of angiogenic sprouts, but never in MCs (Fig. 6A). Dll4-Notch signaling was inhibited using a neutralizing Dll4-Ab (Yamanda et al., 2009). The inhibitory effect was confirmed by downregulation of *Hey2*, a Notch downstream target gene (Fig. 6B). In the aortic ring assay, Dll4-Ab treatment resulted in morphological changes with increased vessel branching and total sprout length (see Fig. S5A in the supplementary material), resembling the vascular phenotype in the retina and tumors of Dll4-mutant mice (Noguera-Troise et al., 2006; Hellstrom et al., 2007; Suchting et al., 2007).

In parametrical analysis, Dll4-Ab treatment enhanced vessel elongation with a concomitant increase in the EC number in each branch in the presence of VEGF (Fig. 6D,E), but did not affect the pattern of tip cell overtaking (Fig. 6C). The increase in vessel elongation was due to increased mean elongation drive without changes in mean tip duration (Fig. 6D). Dll4-Ab treatment also affected stalk cell behavior: mean EC velocity was increased at junctions and stalks, and the 'still' cell population was decreased, whereas other parameters were not changed by Dll4-Ab treatment (Fig. 6F). Increases in vessel elongation and mean velocity of ECs were also obvious in moving images (see Movie 7 in the supplementary material).

Dll4-Notch signaling was also inhibited by treatment with DAPT (Hellstrom et al., 2007; Suchting et al., 2007). This inhibitory effect was confirmed by downregulation of *Hes1*, another Notch downstream target gene (Fig. 6B). In addition, DAPT treatment eventually reduced Dll4 protein in ECs, suggesting inhibition Notch signaling was occurring (Jakobsson et al., 2010) (Fig. 6A). DAPT treatment enhanced branching formation in the same way as Dll4-Ab treatment, although there was no change in the total length of angiogenic sprouts, and sprouts were also wider, reflecting in vivo morphological changes induced by DAPT (see Fig. S5B in the supplementary material) (Hellstrom et al., 2007; Suchting et al., 2007). In parametrical analysis, unexpectedly, DAPT treatment recapitulated only the two Dll4-Ab-induced parametric changes in mean EC velocity and directional motility profiles (Fig. 6C-F; see Movie 8 in the supplementary material). Comparisons of parametric changes between Dll4-Ab and DAPT treatments are summarized in Table 1. The parametric similarities clearly suggest that the Dll4-Notch signaling pathway negatively regulates mean velocity in collective EC movements at stalks and junctions.

Role of EC-MC interaction in collective EC movement driving angiogenic morphogenesis

DAPT can inhibit not only Notch signaling (Hellstrom et al., 2007; Suchting et al., 2007) but also other γ-secretase-dependent pathways (Boulton et al., 2008), some of which are involved in interplays between EC and MC (Gaengel et al., 2009; Liu et al., 2009). Indeed, the number of $NG2^+$, Ednra-$EGFP^+$ MCs covering endothelial sprouts was decreased (Fig. 7A). To test whether the differences between the effects of Dll4-Ab and DAPT are attributable to Dll4-independent EC-MC interactions, the cells were treated with PDGFRβ-Ab, which interrupts proper covering of endothelial sprouts by MCs and the resulting EC-MC interactions (Uemura et al., 2002; Jin et al., 2008; Liu et al., 2009). As expected, the association between ECs and $NG2^+$, Ednra-$EGFP^+$ MCs was diminished by PDGFRβ-Ab, while endothelial sprouting was evident (Fig. 7A). Interestingly, moving images showed that PDGFRβ-Ab treatment apparently increased ECs moving in the direction opposite branch elongation, resulting in retarded branch elongation (see Movie 9 in the supplementary material). Accordingly, parametric analysis revealed that both mean tip duration and elongation drive were decreased by PDGFRβ-Ab treatment with a preserved pattern of tip cell overtaking (Fig. 7B,C). In addition, PDGFRβ-Ab treatment increased retrograde directional motility and decreased the orientation index without changes in velocity or coordination (Fig. 7D), indicating disturbed directional movement. These results recapitulated a portion of the DAPT-induced parametric changes, which had not been observed with Dll4-Ab (Table 1). The similarities in parametrical changes between PDGFRβ-Ab and DAPT suggest that MCs may affect behaviors of tip cells and directed migration at stalks with collective EC movement in a γ-secretase-dependent manner. However, the parametrical changes in response to DAPT treatment might also be due to alterations of EC-EC interplay via γ-secretase-dependent pathways other than the Dll4-Notch pathway.

Molecular and cellular mechanisms driving vessel elongation

Relationships between parametrical changes and the angiogenic factors studied herein are summarized in Fig. 7E. To identify which compartment of the collective EC movement most efficiently contributes to branch elongation, we analyzed correlations between the vessel elongation index and other parameters. Preliminary analyses highlighted elongation drive and velocity at junctions as possible positive explanatory variables and retrograde directional motility as a possible negative explanatory variable (see Fig. S6B,C in the supplementary material). Then, we tested whether the above three parameters can explain vessel elongation by using a multi-regression model. The results suggested elongation drive, velocity at junctions and retrograde directional motility to be significant determinants of vessel elongation in the present setting (Fig. 7F).

Therefore, the parametrical analyses collectively suggested a model possibly explaining the molecular and cellular mechanisms underlying branch elongation (Fig. 7G); VEGF induces vessel elongation by enhancing the elongation drive, velocity and percentage of anterograde directional motility, with elongation drive and velocity being counteracted by Dll4-Notch signaling. MCs may act on ECs to promote elongation drive at the tip and the directional motility that drives branch elongation.

DISCUSSION

Herein, we established a system for spatiotemporally assessing collective EC movements involved in in vitro angiogenesis using live-cell imaging with time-lapse microscopy and computational analysis. This system revealed complex and heterogeneous EC behaviors during angiogenesis: individual ECs migrate forwards and backwards at different velocities, changing their relative positions within the branch network ('cell-mixing'), even at the tip ('overtaking of the tip cell'). Based on an EC-tracking analysis of murine retina, the 'cell-mixing' phenomenon also very likely to occur during in vivo angiogenesis. Parametrical and statistical analyses further demonstrated the molecular and cellular mechanisms underlying collective EC movement. EC-EC interplay via Dll4-Notch signaling counteracts VEGF-induced tip cell elongation and

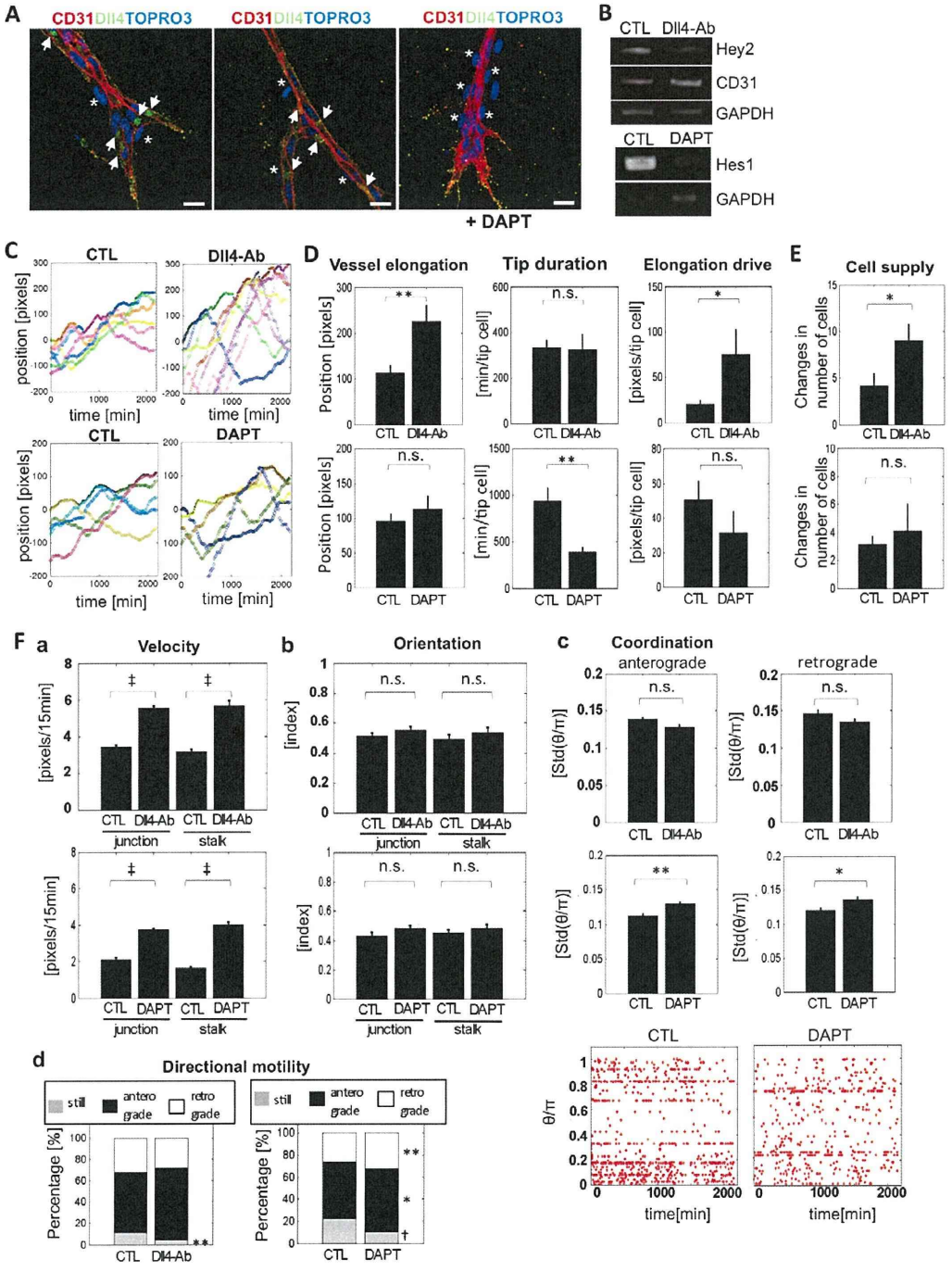

Fig. 6. Dll4-Notch signaling between ECs affects collective EC movements driving vessel elongation. (**A**) Whole-mount double staining of aortic ring assays with or without DAPT treatment. Nuclei were stained with TOPRO3. Dll4 was detected as a lump (arrows) in CD31$^+$ ECs not only at the tip (left panel) but also at the stalk (middle panel), but never in MCs (asterisks). Levels of Dll4 protein in ECs were reduced by DAPT treatment. Scale bars: 25 μm. (**B**) RT-PCR revealed Hey2 and Hes1 expression to be downregulated in cells treated with Dll4-Ab or DAPT, respectively. (**C**) Representative trajectories of tip cells. (**D**) Parameters related to tip cells. (**E**) Cell supply. (**F**) Parameters at junctions and stalks. (a) EC velocity. (b) Orientation. (c) Coordination. Scattered plots show representative of coordination analysis data. (d) Directional motility. See Movies 7 and 8 in the supplementary material. Data are presented as mean±s.e.m. *P<0.05, **P<0.01, $^{\dagger}P$<0.001, $^{\ddagger}P$<0.0001. CTL indicates control.

directed migration. In addition, EC-MC interplay might positively regulate the EC elongation and directional motility, implying a novel role of MCs in the early stage of angiogenesis.

The 'cell-mixing' phenomenon during angiogenesis was unexpected because angiogenic elongation was assumed to be a quasi-static phenomenon in which tip cells with filopodia lead the

Table 1. Effects of Dll4-Ab, DAPT and PDGFRβ-Ab treatments for analyzed parameters

Structure	Parameter	Dll4-Ab	DAPT	PDGFRβ-Ab
Tip	Vessel elongation	↑	→	↓ or →
	Tip duration	→	↓	↓
	Elongation drive	↑	↓ or →	↓
Junction and stalk	Velocity	↑	↑	→
	Orientation	→	→	↓ or →
	Coordination	→	↓	→
	Anterograde motility	→	↑	→
	Retrograde motility	→	↑	↑
	No motility	↓	↓	→

Arrows ↑, ↓ and → indicate significant increase, significant decrease and no change in each parameter, respectively.

way as pioneer cells and a chain of followers serve as stalk cells, which are connected to each other by cell-cell junctions, elongating the sprout via proliferation (Holderfield and Hughes, 2008; De Smet et al., 2009). The present findings indicate that the two distinct cellular phenotypes, tip and stalk, are interchangeable and branches elongate via a mixture of migratory ECs supplied from upstream vascular beds. Accordingly, gene expression patterns characteristic of tip and stalk cells (Phng and Gerhardt, 2009) may depend on positional context within an elongating branch. As for the phenomenon of tip cell overtaking, Jakobsson et al. reported similar findings in both in vitro and in vivo settings (Jakobsson et al., 2010) while we were preparing this manuscript. Taken together with theirs, our findings strongly suggest that cellular behaviors during angiogenesis may be more variable and complex than previously thought.

What is the biological significance of overtaking of tip cell? After one overtaking event, the new tip cell slows and elongation stops after a while, and the cell is then overtaken by the next one, leading us to speculate that the major role of a tip cell may be not only to elongate in itself but also to create a milieu suitable for the next cell. ECs express various matrix metalloproteinases which degrade the surrounding extracellular matrix (ECM) and thereby create space for invasion (van Hinsbergh and Koolwijk, 2008). Furthermore, a recent report (del Toro et al., 2010) on murine retinal neovessels showed that genes involved in ECM remodeling, such as urokinase-plasminogen-activated receptor and nidogen 2, were enriched in the tip cells. Indeed, a tip cell seems to serve as a 'rail' for the following new cell, and this machinery may also explain the 'cell-mixing' phenomenon observed at stalks and junctions.

Interestingly, some ECs migrated backwards when the branch was elongating forwards. Previous reports have shown that gradients of local VEGF appear to provide tip cell migration directionality in the retina (Stone et al., 1995; Provis et al., 1997; Gerhardt et al., 2003). Because the local VEGF gradient would presumably be canceled with addition of a large amount of VEGF to the culture medium in our experimental system, retrograde EC movement may merely reflect a loss of the VEGF gradient. However, administration of VEGF resulted in increased anterograde EC migration at stalks without any gradient. This suggests that there is an additional force driving movement towards the tip. In fact, the present parametrical analysis showed that inhibition of both Dll4-Notch signaling and EC-MC interaction also affected the directionality of EC migration. Thus, mechanisms determining directionality are complex, and VEGF may function to enhance directional movement independently of its regional gradient. At the moment, whether the retrograde EC migration occurs in in vivo angiogenesis is unknown. Even though our observations may not represent a physiological phenomenon, they may provide clues to the mechanism responsible for directionality.

The present results provide clues as to how the spatiotemporal regulation of molecular interactions collectively affect EC behaviors, resulting in branch elongation. The VEGFR-Dll4-Notch circuit is reported to be crucial for tip cell function (Hellstrom et al., 2007; Suchting et al., 2007). Similarly, in the present study, interrupting VEGF and Dll4-Notch signaling pathways affected tip cell behavior, as analyzed by the 'elongation drive' index. More recently, Jakobsson et al. demonstrated that the signal circuit contributes to tip cell selection and the resultant tip cell replacement (Jakobsson et al., 2010). In the present study, however, the frequency of tip overtaking was unchanged regardless of the absence or presence of VEGF or inhibition of Dll4-Notch signaling. Our results imply that another mechanism may drive overtaking of the tip cell. The parametric analysis results suggest γ-secretase-dependent machinery other than the Dll4-Notch pathway and/or EC-MC interplay possibly to control the frequency of tip cell overtaking.

In conjugation with tip cell navigation, migratory behaviors of ECs following the tip cell affected branch elongation as previously assumed (Schmidt et al., 2007; Perryn et al., 2008). VEGF enhanced the velocity and directionality of EC migratory behaviors, resulting in efficient branch elongation, whereas Dll4-Notch signaling exerted inhibitory actions on both. The string of inhibitory actions exerted by the Dll4-Notch pathway may be due to downregulation of VEGFR2 (Ridgway et al., 2006; Williams et al., 2006). Another possibility is that Notch activation might inhibit EC migration via an Id1-dependent mechanism, which potently contributes to angiogenesis (Itoh et al., 2004; Nishiyama et al., 2005). Considering the mosaic expression pattern of Dll4 throughout angiogenic sprouts, Dll4-Notch interactions occur widely between ECs within sprouts, and scattered activation of the Dll4-Notch signal seems to partially explain the heterogeneity of EC movements. Collectively, these results raise the possibility of a yet-to-be defined role of the Dll4-Notch signaling pathway in controlling EC movements at stalks and junctions.

The present study demonstrated that EC-MC interaction might affect collective EC movement driving branch elongation. In particular, the suppressive action on backwards EC movement was marked. MCs are widely accepted as playing a pivotal role in the process of vessel maturation and remodeling at the late stage of angiogenesis. However, the biological significance of MCs in the early stage remained largely unknown, despite MCs having identified in proximity to sprouting ECs during angiogenesis of the developing brain and retina (Bauer et al., 1992; Ozerdem and Stallcup, 2003). Therefore, this observation suggests a novel role

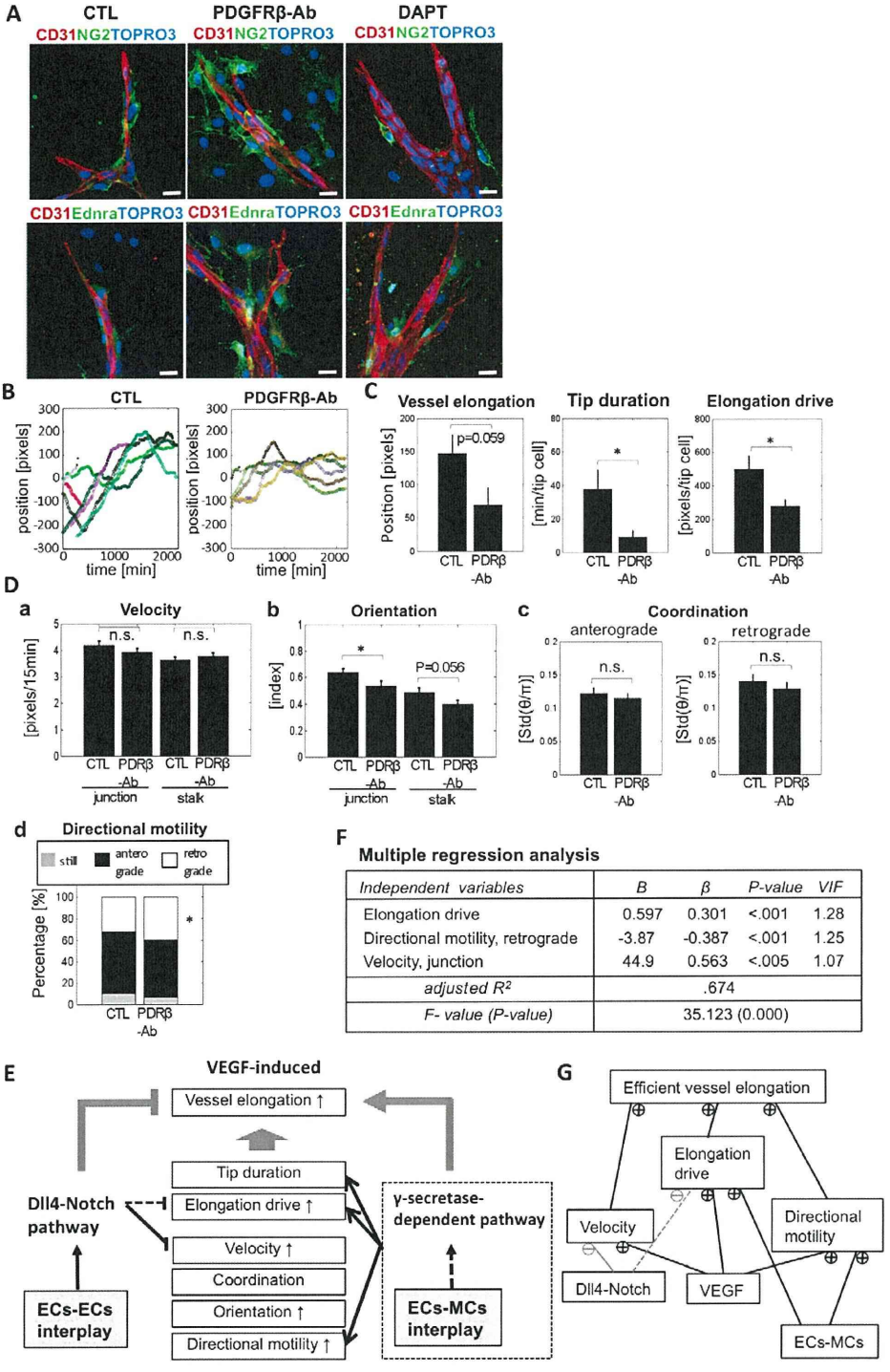

Fig. 7. Molecular and cellular mechanisms for vessel elongation by EC-EC and EC-MC interactions. Time-lapse imaging was performed in murine aortic ring assays with PDGFRβ-Ab treatment. (**A**) Whole-mount staining in the assay using the wild-type or *Ednra*^{egfp} mouse with the indicated treatment. Nuclei were stained with TOPRO3. Scale bars: 25 μm. (**B**) Representative trajectories of tip cells. (**C**) Parameters related to tip cells. (**D**) Parameters at junctions and stalks. (a) EC velocity. (b) Orientation. (c) Coordination. (d) Directional motility. PDGFRβ-Ab treatment tended to decrease vessel elongation, while clearly decreasing elongation drive and tip duration. See also Movie 9 in the supplementary material. Data are presented as mean±s.e.m. *P<0.05. CTL and PDR-β indicate control and PDGFRβ, respectively. (**E**) The summary of parametrical changes and their underlying molecular pathways. (**F**) Multi-regression analysis. *B*, unstandardized coefficient; β, standardized coefficient; *VIF*, variance inflation factor. (**G**) A possible model explaining molecular and cellular mechanisms underlying vessel elongation. Minus marks and gray indicate inhibitory effects.

for MCs in angiogenesis. The present study further indicated that a γ-secretase-dependent pathway other than the Dll4-Notch pathway might contribute to the EC-MC interplay. γ-Secretase activates the Notch signal via cleavage of its receptor and a jagged 1 ligand is expressed in MCs (Domenga et al., 2004; Liu et al., 2009). γ-Secretase activity also regulates the dynamics of cadherins (Boulton et al., 2008), which mediate morphogenetic movements (Gumbiner, 2005; Theveneau et al., 2010). Thus, MCs may use the jagged 1-Notch pathway and/or the cadherin-mediated cell-adhesion system for the interplay with ECs, resulting in the control of collective EC movements during angiogenesis.

In conclusion, we have developed a time-lapse imaging and quantitative analysis system revealing cell-based mechanisms underlying elongation processes during in vitro angiogenesis. The physiological relevance of 'cell mixing', one of our major findings, was confirmed by analysis of in vivo retinal angiogenesis. The biological findings reported herein and the parameters that we defined can be incorporated in an agent-based model to simulate angiogenic cell behavior, which may in turn yield new insights for understanding the sprouting, elongating and branching aspects of angiogenesis. Furthermore, the methodology employed may allow the gaps among molecular, cellular and integrative bases of organic morphogenesis to be bridged.

Acknowledgements
We thank Olympus Corporation for multiple trials on FluoView FV10i, Dr Shin-ichi Nishikawa and Dr Akiyoshi Uemura for antibodies, and Dr Hideyuki Sakoda for the adenovirus. We also thank Yuko Fujisawa, Takahiro Sato, Rieko Asai and Sakura Kushiyama for excellent technical assistance. MTrackJ was developed at the Biomedical Imaging Group Rotterdam of the Erasmus MC-University Medical Center Rotterdam (The Netherlands) by Erik Meijering.

Funding
This work was supported in part by the Global COE Program (Integrative Life Science Based on the Study of Biosignaling Mechanisms) from the Ministry of Education, Culture, Sports, Science and Technology (MEXT, Japan); by grants-in-aid for scientific research from MEXT (Japan) [23111505 to K.N.]; by grants-in-aid for scientific research from the Ministry of Health, Labour and Welfare of Japan [09156294 to H.K.]; and by grants-in-aid for scientific research from Japan Society for the Promotion of Science (JSPS, Japan) [23591099 to K.N., 21390238 to H.K.].

Competing interests statement
The authors declare no competing financial interests.

Supplementary material
Supplementary material for this article is available at
http://dev.biologists.org/lookup/suppl/doi:10.1242/dev.068023/-/DC1

References

Armulik, A., Abramsson, A. and Betsholtz, C. (2005). Endothelial/pericyte interactions. *Circ. Res.* **97**, 512-523.
Asai, R., Kurihara, Y., Fujisawa, K., Sato, T., Kawamura, Y., Kokubo, H., Tonami, K., Nishiyama, K., Uchijima, Y., Miyagawa-Tomita, S. et al. (2010). Endothelin receptor type A expression defines a distinct cardiac subdomain within the heart field and is later implicated in chamber myocardium formation. *Development* **137**, 3823-3833.
Bauer, H. C., Steiner, M. and Bauer, H. (1992). Embryonic development of the CNS microvasculature in the mouse: new insights into the structural mechanisms of early angiogenesis. *EXS* **61**, 64-68.
Blacher, S., Devy, L., Burbridge, M. F., Roland, G., Tucker, G., Noel, A. and Foidart, J. M. (2001). Improved quantification of angiogenesis in the rat aortic ring assay. *Angiogenesis* **4**, 133-142.
Boulton, M. E., Cai, J. and Grant, M. B. (2008). gamma-Secretase: a multifaceted regulator of angiogenesis. *J. Cell. Mol. Med.* **12**, 781-795.
Claxton, S. and Fruttiger, M. (2004). Periodic Delta-like 4 expression in developing retinal arteries. *Gene Expr. Patterns* **5**, 123-127.
Dai, J., Sultan, S., Taylor, S. S. and Higgins, J. M. (2005). The kinase haspin is required for mitotic histone H3 Thr 3 phosphorylation and normal metaphase chromosome alignment. *Genes Dev.* **19**, 472-488.
De Smet, F., Segura, I., De Bock, K., Hohensinner, P. J. and Carmeliet, P. (2009). Mechanisms of vessel branching: filopodia on endothelial tip cells lead the way. *Arterioscler. Thromb. Vasc. Biol.* **29**, 639-649.
del Toro, R., Prahst, C., Mathivet, T., Siegfried, G., Kaminker, J. S., Larrivee, B., Breant, C., Duarte, A., Takakura, N., Fukamizu, A. et al. (2010). Identification and functional analysis of endothelial tip cell-enriched genes. *Blood* **116**, 4025-4033.
Domenga, V., Fardoux, P., Lacombe, P., Monet, M., Maciazek, J., Krebs, L. T., Klonjkowski, B., Berrou, E., Mericskay, M., Li, Z. et al. (2004). Notch3 is required for arterial identity and maturation of vascular smooth muscle cells. *Genes Dev.* **18**, 2730-2735.
Friedl, P. and Gilmour, D. (2009). Collective cell migration in morphogenesis, regeneration and cancer. *Nat. Rev. Mol. Cell Biol.* **10**, 445-457.
Gaengel, K., Genove, G., Armulik, A. and Betsholtz, C. (2009). Endothelial-mural cell signaling in vascular development and angiogenesis. *Arterioscler. Thromb. Vasc. Biol.* **29**, 630-638.
Gerhardt, H., Golding, M., Fruttiger, M., Ruhrberg, C., Lundkvist, A., Abramsson, A., Jeltsch, M., Mitchell, C., Alitalo, K., Shima, D. et al. (2003). VEGF guides angiogenic sprouting utilizing endothelial tip cell filopodia. *J. Cell Biol.* **161**, 1163-1177.
Gumbiner, B. M. (2005). Regulation of cadherin-mediated adhesion in morphogenesis. *Nat. Rev. Mol. Cell Biol.* **6**, 622-634.
Hellstrom, M., Gerhardt, H., Kalen, M., Li, X., Eriksson, U., Wolburg, H. and Betsholtz, C. (2001). Lack of pericytes leads to endothelial hyperplasia and abnormal vascular morphogenesis. *J. Cell Biol.* **153**, 543-553.
Hellstrom, M., Phng, L. K., Hofmann, J. J., Wallgard, E., Coultas, L., Lindblom, P., Alva, J., Nilsson, A. K., Karlsson, L., Gaiano, N. et al. (2007). Dll4 signalling through Notch1 regulates formation of tip cells during angiogenesis. *Nature* **445**, 776-780.
Hendzel, M. J., Wei, Y., Mancini, M. A., Van Hooser, A., Ranalli, T., Brinkley, B. R., Bazett-Jones, D. P. and Allis, C. D. (1997). Mitosis-specific phosphorylation of histone H3 initiates primarily within pericentromeric heterochromatin during G2 and spreads in an ordered fashion coincident with mitotic chromosome condensation. *Chromosoma* **106**, 348-360.
Hofmann, J. J. and Luisa Iruela-Arispe, M. (2007). Notch expression patterns in the retina: an eye on receptor-ligand distribution during angiogenesis. *Gene Expr. Patterns* **7**, 461-470.
Holderfield, M. T. and Hughes, C. C. (2008). Crosstalk between vascular endothelial growth factor, notch, and transforming growth factor-beta in vascular morphogenesis. *Circ. Res.* **102**, 637-652.
Itoh, F., Itoh, S., Goumans, M.-J., Valdimarsdottir, G., Iso, T., Dotto, G. P., Hamamori, Y., Kedes, L., Kato, M. and ten Dijke, P. (2004). Synergy and antagonism between Notch and BMP receptor signaling pathways in endothelial cells. *EMBO J.* **23**, 541-551.
Jakobsson, L., Franco, C. A., Bentley, K., Collins, R. T., Ponsioen, B., Aspalter, I. M., Rosewell, I., Busse, M., Thurston, G., Medvinsky, A. et al. (2010). Endothelial cells dynamically compete for the tip cell position during angiogenic sprouting. *Nat. Cell Biol.* **12**, 943-953.
Jin, S., Hansson, E. M., Tikka, S., Lanner, F., Sahlgren, C., Farnebo, F., Baumann, M., Kalimo, H. and Lendahl, U. (2008). Notch signaling regulates platelet-derived growth factor receptor-beta expression in vascular smooth muscle cells. *Circ. Res.* **102**, 1483-1491.
Lafleur, M. A., Forsyth, P. A., Atkinson, S. J., Murphy, G. and Edwards, D. R. (2001). Perivascular cells regulate endothelial membrane type-1 matrix metalloproteinase activity. *Biochem. Biophys. Res. Commun.* **282**, 463-473.
Liu, H., Kennard, S. and Lilly, B. (2009). NOTCH3 expression is induced in mural cells through an autoregulatory loop that requires endothelial-expressed JAGGED1. *Circ. Res.* **104**, 466-475.
Montell, D. J. (2008). Morphogenetic cell movements: diversity from modular mechanical properties. *Science* **322**, 1502-1505.
Murakami, T., Suzuma, K., Takagi, H., Kita, M., Ohashi, H., Watanabe, D., Ojima, T., Kurimoto, M., Kimura, T., Sakamoto, A. et al. (2006). Time-lapse imaging of vitreoretinal angiogenesis originating from both quiescent and mature vessels in a novel ex vivo system. *Invest. Ophthalmol. Vis. Sci.* **47**, 5529-5536.
Nishiyama, K., Takaji, K., Kataoka, K., Kurihara, Y., Yoshimura, M., Kato, A., Ogawa, H. and Kurihara, H. (2005). Id1 gene transfer confers angiogenic property on fully differentiated endothelial cells and contributes to therapeutic angiogenesis. *Circulation* **112**, 2840-2850.
Noguera-Troise, I., Daly, C., Papadopoulos, N. J., Coetzee, S., Boland, P., Gale, N. W., Lin, H. C., Yancopoulos, G. D. and Thurston, G. (2006). Blockade of Dll4 inhibits tumour growth by promoting non-productive angiogenesis. *Nature* **444**, 1032-1037.
Ozerdem, U. and Stallcup, W. B. (2003). Early contribution of pericytes to angiogenic sprouting and tube formation. *Angiogenesis* **6**, 241-249.
Ozerdem, U., Grako, K. A., Dahlin-Huppe, K., Monosov, E. and Stallcup, W. B. (2001). NG2 proteoglycan is expressed exclusively by mural cells during vascular morphogenesis. *Dev. Dyn.* **222**, 218-227.

Perryn, E. D., Czirok, A. and Little, C. D. (2008). Vascular sprout formation entails tissue deformations and VE-cadherin-dependent cell-autonomous motility. *Dev. Biol.* **313**, 545-555.
Phng, L. K. and Gerhardt, H. (2009). Angiogenesis: a team effort coordinated by notch. *Dev. Cell* **16**, 196-208.
Provis, J. M., Leech, J., Diaz, C. M., Penfold, P. L., Stone, J. and Keshet, E. (1997). Development of the human retinal vasculature: cellular relations and VEGF expression. *Exp. Eye Res.* **65**, 555-568.
Ridgway, J., Zhang, G., Wu, Y., Stawicki, S., Liang, W. C., Chanthery, Y., Kowalski, J., Watts, R. J., Callahan, C., Kasman, I. et al. (2006). Inhibition of Dll4 signalling inhibits tumour growth by deregulating angiogenesis. *Nature* **444**, 1083-1087.
Schmidt, M., Paes, K., De Maziere, A., Smyczek, T., Yang, S., Gray, A., French, D., Kasman, I., Klumperman, J., Rice, D. S. et al. (2007). EGFL7 regulates the collective migration of endothelial cells by restricting their spatial distribution. *Development* **134**, 2913-2923.
Siekmann, A. F. and Lawson, N. D. (2007). Notch signalling limits angiogenic cell behaviour in developing zebrafish arteries. *Nature* **445**, 781-784.
Stone, J., Itin, A., Alon, T., Pe'er, J., Gnessin, H., Chan-Ling, T. and Keshet, E. (1995). Development of retinal vasculature is mediated by hypoxia-induced vascular endothelial growth factor (VEGF) expression by neuroglia. *J. Neurosci.* **15**, 4738-4747.
Suchting, S., Freitas, C., le Noble, F., Benedito, R., Breant, C., Duarte, A. and Eichmann, A. (2007). The Notch ligand Delta-like 4 negatively regulates endothelial tip cell formation and vessel branching. *Proc. Natl. Acad. Sci. USA* **104**, 3225-3230.
Theveneau, E., Marchant, L., Kuriyama, S., Gull, M., Moepps, B., Parsons, M. and Mayor, R. (2010). Collective chemotaxis requires contact-dependent cell polarity. *Dev. Cell* **19**, 39-53.
Uemura, A., Ogawa, M., Hirashima, M., Fujiwara, T., Koyama, S., Takagi, H., Honda, Y., Wiegand, S. J., Yancopoulos, G. D. and Nishikawa, S. (2002). Recombinant angiopoietin-1 restores higher-order architecture of growing blood vessels in mice in the absence of mural cells. *J. Clin. Invest.* **110**, 1619-1628.
van Hinsbergh, V. W. and Koolwijk, P. (2008). Endothelial sprouting and angiogenesis: matrix metalloproteinases in the lead. *Cardiovasc. Res.* **78**, 203-212.
Vitorino, P. and Meyer, T. (2008). Modular control of endothelial sheet migration. *Genes Dev.* **22**, 3268-3281.
Williams, C. K., Li, J. L., Murga, M., Harris, A. L. and Tosato, G. (2006). Up-regulation of the Notch ligand Delta-like 4 inhibits VEGF-induced endothelial cell function. *Blood* **107**, 931-939.
Yamanda, S., Ebihara, S., Asada, M., Okazaki, T., Niu, K., Ebihara, T., Koyanagi, A., Yamaguchi, N., Yagita, H. and Arai, H. (2009). Role of ephrinB2 in nonproductive angiogenesis induced by Delta-like 4 blockade. *Blood* **113**, 3631-3639.
Yamashita, J., Itoh, H., Hirashima, M., Ogawa, M., Nishikawa, S., Yurugi, T., Naito, M. and Nakao, K. (2000). Flk1-positive cells derived from embryonic stem cells serve as vascular progenitors. *Nature* **408**, 92-96.

Angiogenic morphogenesis driven by dynamic and heterogeneous collective endothelial cell movement

DEV068023 Supplementary Material

Files in this Data Supplement:

Supplemental Table S1 -

Supplemental Figure S1 -

Fig. S1. Selective marking of ECs by staining with SYTO dyes. (A,B) Serial confocal images along the z-axis (A) and a z-stack image (B) of live cells immunostained for CD31 and PDGFRß with nuclear SYTO dye staining in a murine aortic ring assay. ECs (CD31+) were more strongly stained with SYTO-16 than were MCs (CD31- PDGFRß+). (C) Distinct localization of SYTO-61 and Ednra-EGFP signals in a murine aortic ring assay using Ednraegfp mouse. EGFP signals are detected only in CD31+ MCs (asterisks) (see also Movie 2 in the supplementary material). (D) Flow cytometry analysis showing preferential SYTO-61 staining for CD31+, Ednra-EGFP− ECs. Scale bars: 25 μm.

Supplemental Figure S2 -

Fig. S2. The percentage of ECs undergoing mitosis in in vitro and in vivo angiogenesis. (A) An example of ECs undergoing mitosis observed in time-lapse live imaging of a murine aortic ring assay. Nuclei were stained with SYTO-16 dye. Red arrows indicate an event of mitosis. (B) Mitotic ECs were detected by staining for PH3 in a murine aortic ring assay and murine retinal neovessels at P1 and P3. The rate of PH3+ ECs to total ECs was quite low equally among the three groups. (C) The rate of PH3+ ECs was compared between distal and proximal regions. PH3+ ECs (arrows) were detected more frequently in the distal region, including the tip, than in more proximal regions in a murine aortic ring assay, as well as in murine retinal angiogenesis. Solid and broken lines indicate subareas referred to as □distal 400□ and □proximal□, respectively.

Supplemental Figure S3 -

Fig. S3. An example of the trajectory analysis. Trajectory of the EC indicated by red arrows in Fig. 2A is shown. Nuclear positions were orthogonally projected to the axis of elongation (white arrow), which corresponds to the direction of the tip migration. The vertical axis is the position of each cell (pixels) and the horizontal axis is time (minutes). Zero position of the vertical axis indicates the position of the base of the branch. The trajectory of the tip was drawn in thick black. Using the nuclear coordinates extracted from confocal images obtained by tracking the cell nuclei, a trajectory of the individual cell can be re-drawn in an elongating branch. The EC (yellow trajectory) migrates to the

tip with relatively high speed compared with one of branch elongation.

Supplemental Figure S4 -

Fig. S4. Identification of "cell-mixing" phenomenon during murine retinal angiogenesis in vivo. Murine retinal vasculature was immunostained with CD31 or CD34 at 6 and 12 hours after intravascular injection of BS-1 lectin. (A) Serial confocal images along the z-axis at 6 hours after the injection. Confocal images confirmed that lectin was labeled on the CD31+ ECs (arrowheads). (B) Z-stack confocal images of retinal vasculature 12 hours after the injection. Lectin-labeled ECs (arrowheads) were observed sporadically in the distal regions of CD34+ sprouts (B, part a). Conversely, in more proximal regions, lectin-unlabeled ECs (yellow asterisk indicates an example) were sporadically observed in lectin-labeled sprouts (B, part b). Arrows indicate the direction of vessel elongation. Scale bars: 25 μm.

Supplemental Figure S5 -

Fig. S5. Effects of Dll4-neutralizing and DAPT treatments on the morphology of sprouts in an in vitro angiogenesis. Murine aortic ring assay was performed in the absence (control) or presence of anti-Dll4-antibody (Ab) (A) or DAPT (B). Upper panel, iz-stack images of angiogenic sprouts positive for CD31 at day 7 of the culture. Lower panel, quantitative analyses of morphology changes. Anti-Dll4-Ab treatment increased branch point formation and total length of angiogenic sprouts (A). Similarly, DAPT treatment enhanced branch formation (B). Spouts were wider in DAPT treatment, although there was no change in the total length of angiogenic sprouts. Scale bars: 400 μm. Data are presented as mean±s.e.m. *P<0.05, **P<0.01. CTL indicates control.

Supplemental Figure S6 -

Fig. S6. Single- and multi-regression analysis between vessel elongation and the other parameters for collective EC movement. (A) Parameters at the tip and at the stalk and junction for collective EC movement driving vessel elongation. (B) Single regression analyses between vessel elongation and parameters for collective EC movement were performed. (C) Through the single regression analyses, seven out of 10 parameters for collective EC movement significantly correlated with vessel elongation, and then seven parameters were selected as explanatory variables for vessel elongation in following multi-regression analysis. B, β, and VIF indicate unstandardized coefficient, standardized coefficient and variance inflation factor, respectively.

Movie 1 -

Movie 1. Dynamic behavior of ECs during angiogenic sprouting in mouse aortic ring

assay. Images were taken every 15 minutes for 36 hours. (Left) Merged z-stack images of confocal and phase-contrast views. (Middle) Z-stack confocal images. (Right) Schematic images showing nuclear positions of individual ECs. ECs were clustered 5 to 10 in the same color to show mixing of ECs. Complex and heterogeneous EC movement during angiogenic sprouting was visualized. Some cells move backwards even though the branch is elongating and ECs from proximal ends (vascular bed) participate in forming branches.

Movie 2 -

Movie 2. Distinction between ECs and MCs in the angiogenic sprouts of wild-type (left) and EdnraEGFP (right) mice by nuclear stain with SYTO dyes. Images were taken at the interval of 5 minutes for 5 hours. Nuclei of ECs were strongly stained with SYTO dyes, whereas MC nuclei were only faintly stained. MCs can be identified by their morphology (left) and EGFP signals (right). Fourteen frames were taken every second.

Movie 3 -

Movie 3. Visualization of individual EC behavior in angiogenic sprouts by mosaic analysis. Images were taken every 7 minutes for 9 hours. (Left) Phase-contrast images. (Middle, right) Z-stack confocal images. See Materials and methods for mosaic analysis. An EGFP-labeled EC with lectin (red) (marked with red closed circle) overtakes a tip cell and is then replaced by a follower EC without EGFP signal (marked with yellow closed circles). In addition, a highly motile EC (marked with red circles) displays forward-rear cell polarity, whereas a low motile EC (white arrowhead) displays spindle shape without cell polarity. Blue indicates nuclear stain with SYTO dye. Fourteen frames were taken every second.

Movie 4 -

Movie 4. Visualization of the behavior of individual ECs in angiogenic sprouts by mosaic analysis. Images were taken every 5 minutes for 12 hours. (Left) Phase-contrast images. (Right) Z-stack confocal images. See Materials and methods for mosaic analysis. An EGFP-labeled EC at the tip starts to move in opposite direction against vessel elongation at a certain moment. The cell polarity dynamically changes depending on the moving direction. Blue indicates nuclear stain with SYTO dye. Fourteen frames were taken every second.

Movie 5 -

Movie 5. Visualization of the behavior of individual ECs in angiogenic sprouts by mosaic analysis. (Left) Phase-contrast images. (Right) Z-stack confocal images. See Materials and methods regarding mosaic analysis. An EC (white arrowhead) loses cell

polarity just before being taken over by a follower (red arrowhead); the EC gains cell polarity again at the next moment and starts to move to the tip (yellow arrowhead). Blue indicates nuclear stain with SYTO dye. Fourteen frames were taken every second.

Movie 6 -

Movie 6. Comparison of angiogenesis between different doses of VEGF. Images were taken every 15 minutes for 36 hours. Merged images of z-stack confocal and phase-contrast views. Nuclei were visualized by staining with SYTO dye (green). (Left) VEGF 0 ng/ml. (Right) VEGF 50 ng/ml. With higher VEGF, there is more branch elongation and sprouting out. ECs seem to move more rapidly. Fourteen frames were taken every second.

Movie 7 -

Movie 7. Comparison of angiogenesis between Dll4-Ab (right) and control IgG (left), both with VEGF 50 ng/ml. Images were taken every 15 minutes for 36 hours. Merged images of z-stack confocal and phase-contrast views. Nuclei were visualized by staining with SYTO dye (green). In the images, the nuclei of each EC are pseudocolored. There is excessive elongation in Dll4-Ab group. In addition, ECs seem to move faster as a whole than they do in control settings. Fourteen frames were taken every second.

Movie 8 -

Movie 8. Comparison of angiogenesis between DAPT (right) and control DMSO (left), both with VEGF 50 ng/ml. Images were taken every 15 minutes for 36 hours. (Upper panels) Z-stack confocal images. (Lower panels) Merged images of z-stack confocal and phase-contrast views. Nuclei were visualized by staining with SYTO dye (green). ECs move faster as a whole in the DAPT group than they do in control settings. In addition, more ECs seem to migrate backwards in the DPAT group when the branch is elongating forwards. Fourteen frames were taken every second.

Movie 9 -

Movie 9. Comparison of angiogenesis between PDFGRß-Ab (right) and control IgG (left), both with VEGF 50 ng/ml. This movie relates to Fig. 7. Images were taken every 15 minutes for 36 hours. (Upper panels) Z-stack confocal images. (Lower panels) Merged images of z-stack confocal and phase-contrast views. Nuclei were visualized by staining with SYTO dye (green). More ECs migrate backwards when the branch is elongated forwards in PDFGRß-Ab treatment than they do in control settings, resulting in retarded branch elongation. Fourteen frames were taken every second.

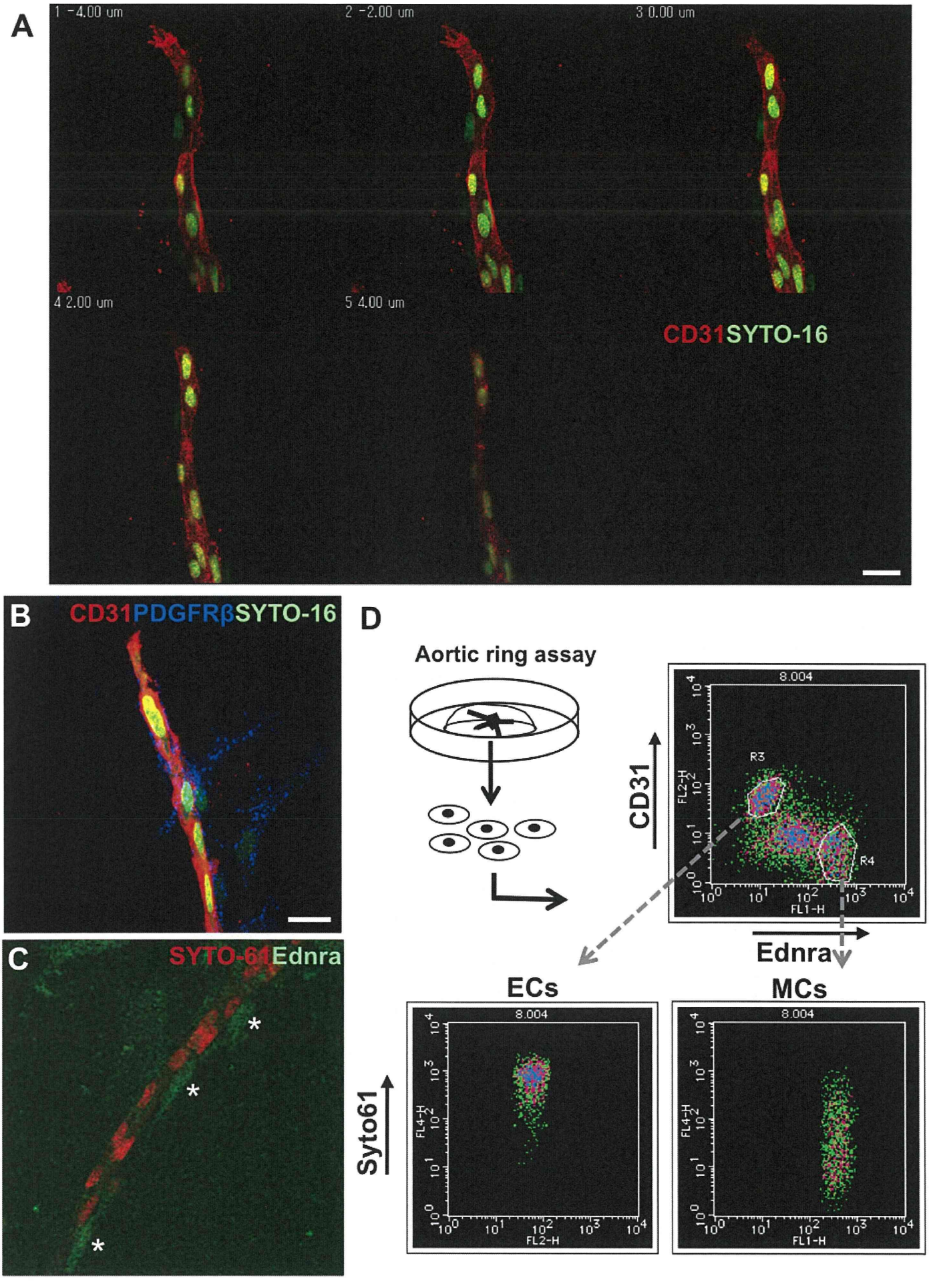
A
1 -4.00 um
2 -2.00 um
3 0.00 um
4 2.00 um
5 4.00 um
CD31SYTO-16
B
CD31PDGFRβSYTO-16
C
SYTO-61Ednra
D
Aortic ring assay
CD31
Ednra
8.004
R3
R4
FL2-H
FL1-H
ECs
MCs
Syto61
FL4-H

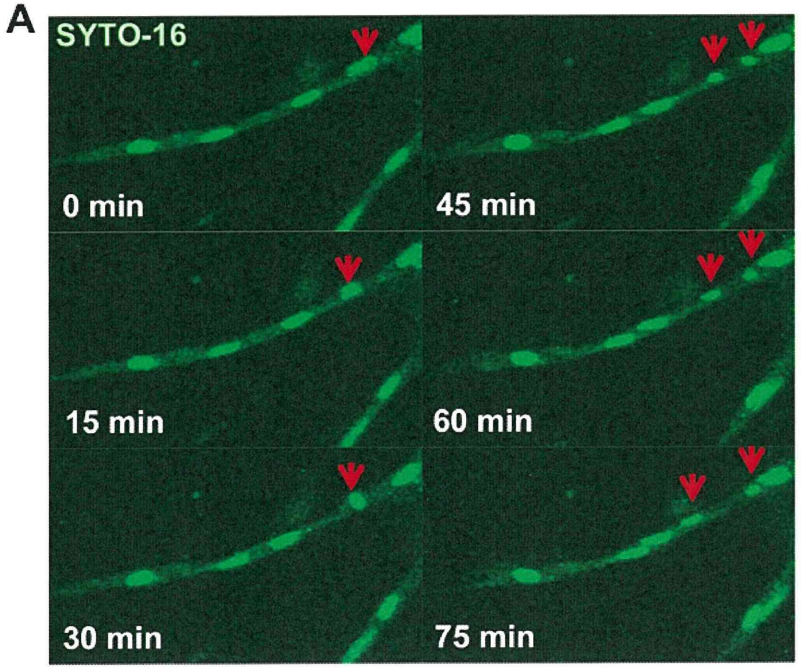
A
SYTO-16
0 min
45 min
15 min
60 min
30 min
75 min

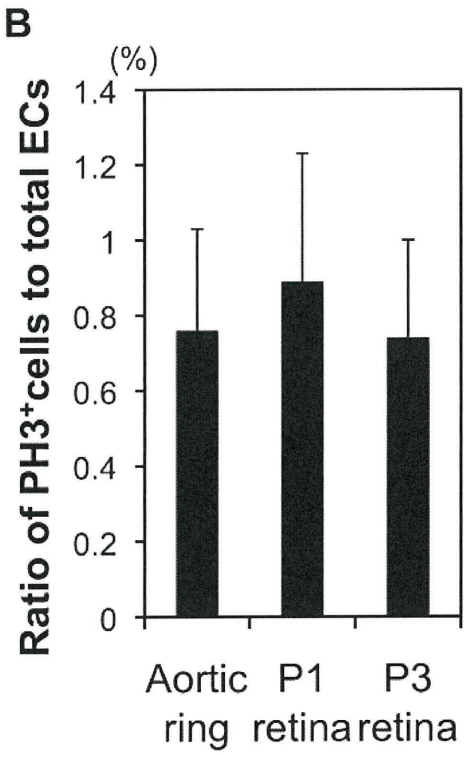
B
(%)
Ratio of PH3+cells to total ECs
1.4
1.2
1
0.8
0.6
0.4
0.2
0
Aortic ring
P1 retina
P3 retina

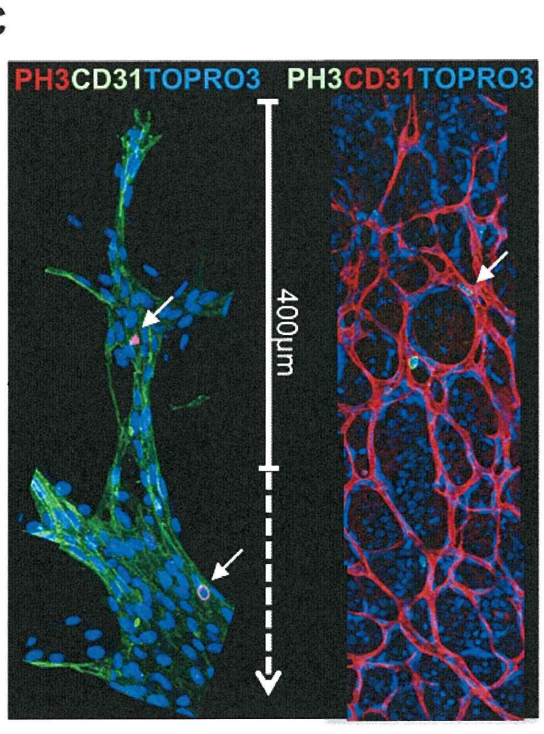
C
PH3CD31TOPRO3
PH3CD31TOPRO3
400μm

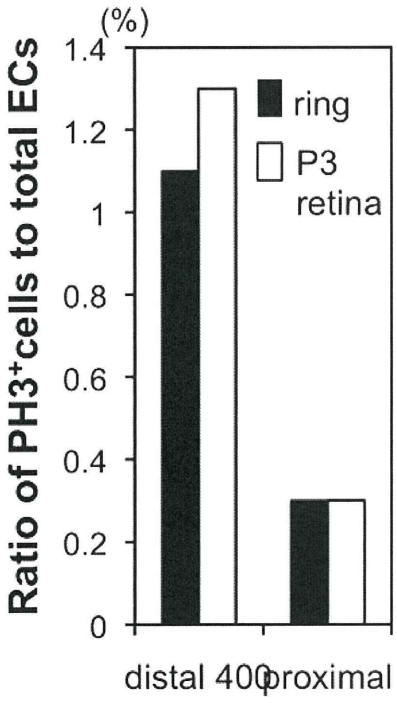
(%)
Ratio of PH3+cells to total ECs
1.4
1.2
1
0.8
0.6
0.4
0.2
0
ring
P3 retina
distal
400
proximal

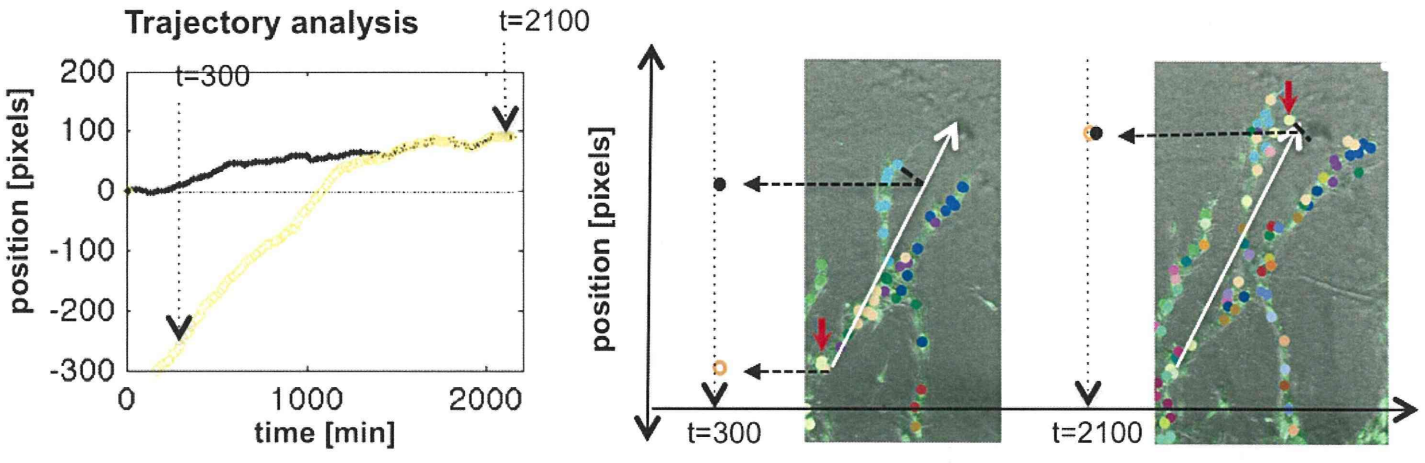
Trajectory analysis
t=2100
t=300
200
100
0
-100
-200
-300
position [pixels]
0
1000
2000
time [min]
position [pixels]
t=300
t=2100

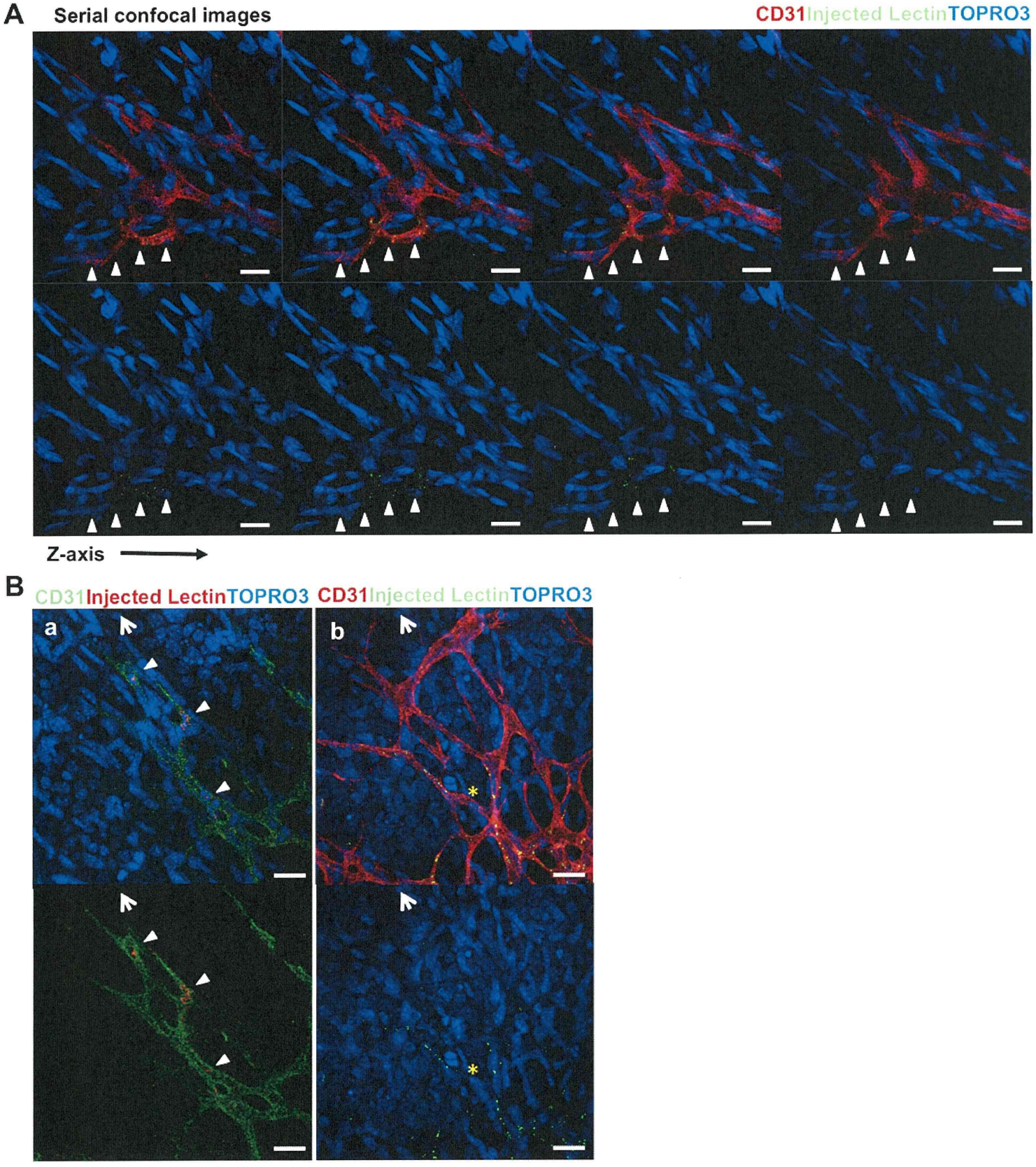
A
Serial confocal images
CD31Injected LectinTOPRO3
Z-axis
B
CD31Injected LectinTOPRO3
CD31Injected LectinTOPRO3
a
b

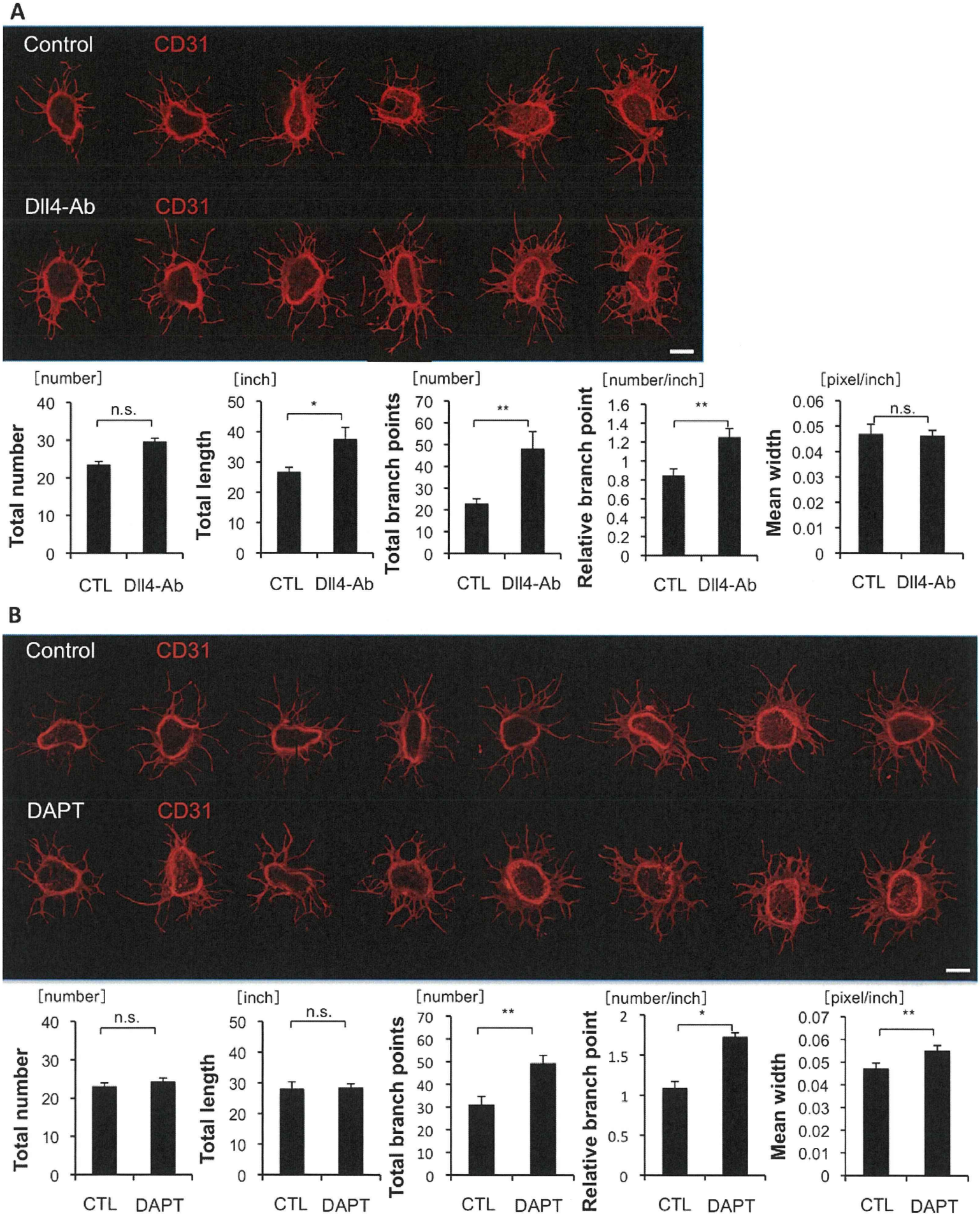
A
Control
CD31
Dll4-Ab
CD31
[number]
Total number
n.s.
CTL
Dll4-Ab
[inch]
Total length
*
CTL
Dll4-Ab
[number]
Total branch points
**
CTL
Dll4-Ab
[number/inch]
Relative branch point
**
CTL
Dll4-Ab
[pixel/inch]
Mean width
n.s.
CTL
Dll4-Ab
B
Control
CD31
DAPT
CD31
[number]
Total number
n.s.
CTL
DAPT
[inch]
Total length
n.s.
CTL
DAPT
[number]
Total branch points
**
CTL
DAPT
[number/inch]
Relative branch point
*
CTL
DAPT
[pixel/inch]
Mean width
**
CTL
DAPT

A

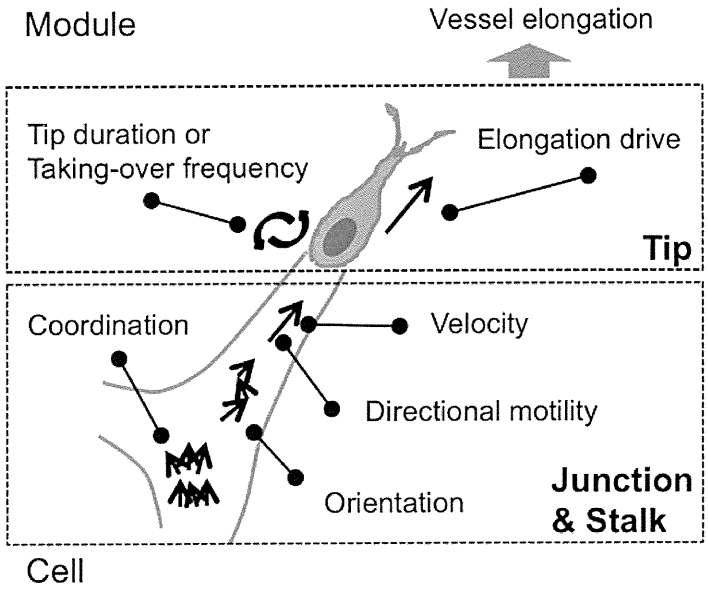

B

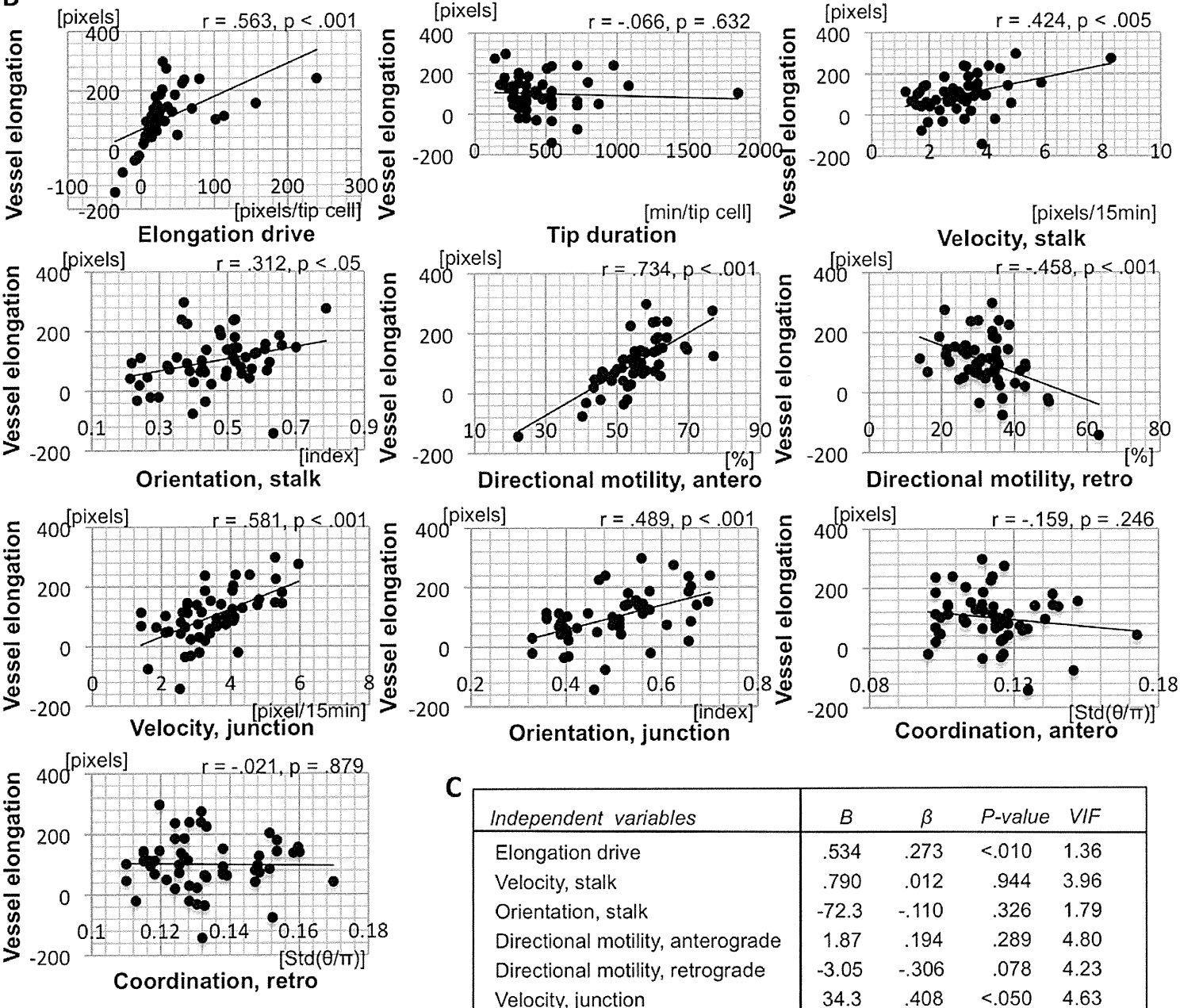

C

Independent variables	*B*	*β*	*P-value*	*VIF*
Elongation drive	.534	.273	<.010	1.36
Velocity, stalk	.790	.012	.944	3.96
Orientation, stalk	-72.3	-.110	.326	1.79
Directional motility, anterograde	1.87	.194	.289	4.80
Directional motility, retrograde	-3.05	-.306	.078	4.23
Velocity, junction	34.3	.408	<.050	4.63
Orientation, junction	88.9	.107	.280	1.42
adjusted R^2	.706			
F- value (P-value)	14.746 (0.000)			

Table S1. The percentage of ECs undergoing mitosis

	Tip*	Stalk**	Bridge†	Junction‡	Sheet§	All/n$	Ratio (%)
VEGF (0 ng/ml)	0	0	0	0	0	0/129	0.0
	0	2	0	0	8	10/233	4.3
	0	0	0	0	0	0/126	0.0
VEGF (5 ng/ml)	0	0	1	0	3	4/245	1.6
	0	0	0	1	1	2 /257	0.8
	0	1	3	4	1	9/217	4.1
VEGF (50 ng/ml)	0	3	2	0	0	5/83	6.0
	0	2	4	3	0	9/211	4.3
	0	0	0	1	1	2/178	1.1

The number of ECs undergoing mitosis at specified places.
*At the tip.
**At blunt-ended regions (including the tip) distal to the junctions.
†At regions connecting two junctions.
‡At regions where two or more stalks diverge or converge.
§At vascular beds where ECs form sheets.
$The total number of ECs observed.

Gene Expression Patterns 11 (2011) 371–377

Contents lists available at ScienceDirect

Gene Expression Patterns

journal homepage: www.elsevier.com/locate/gep

Identification and developmental analysis of endothelin receptor type-A expressing cells in the mouse kidney

Taro Kitazawa [1], Takahiro Sato [1,2], Koichi Nishiyama, Rieko Asai, Yuichiro Arima, Yasunobu Uchijima, Yukiko Kurihara, Hiroki Kurihara *

Department of Physiological Chemistry and Metabolism, Graduate School of Medicine, The University of Tokyo, 7-3-1 Hongo, Bunkyo-ku, Tokyo 113-0033, Japan

ARTICLE INFO

Article history:
Received 7 March 2011
Received in revised form 26 April 2011
Accepted 27 April 2011
Available online 1 May 2011

Keywords:
Endothelin receptor
Kidney
Metanephric mesenchyme
Smooth muscle cell
Juxtaglomerular cell

ABSTRACT

The endothelin (Edn) system plays pleiotropic roles in renal function and various disease processes through two distinct G protein-coupled receptors, Edn receptors type-A (Ednra) and type-B (Ednrb). However, difficulties in the accurate identification of receptor-expressing cells in situ have made it difficult to dissect their diverse action in renal (patho)physiology. We have recently established mouse lines in which *lacZ* and *EGFP* are 'knocked-in' to the *Ednra* locus to faithfully mark *Ednra*-expressing cells. Here we analyzed these mice for their expression in the kidney to characterize *Ednra*-expressing cells. *Ednra* expression was first observed in undifferentiated mesenchymal cells around the ureteric bud at E12.5. Thereafter, *Ednra* expression was widely observed in vascular smooth muscle cells, JG cells and mesenchymal cells in the interstitium. After growth, the expression became confined to vascular smooth muscle cells, pericytes and renin-producing JG cells. By contrast, most cells in the nephron and vascular endothelial cells did not express *Ednra*. These results indicate that *Ednra* expression may be linked with non-epithelial fate determination and differentiation of metanephric mesenchyme. *Ednra-lacZ/EGFP* knock-in mice may serve as a useful tool in studies on renal function and pathophysiology of various renal diseases.

Systemic and local circulatory homeostasis is maintained by a balance between vasoconstrictive and vasodilatory factors. The endothelin (Edn) system, composed of three peptide ligands (Edn1, Edn2 and Edn3) and their two G protein-coupled receptors (endothelin receptors type-A (Ednra) and type-B (Ednrb)), is involved in this mechanism (Masaki, 2004; Yanagisawa et al., 1988). In addition to their vasoconstrictive effects, Edns have a diverse set of biological activities such as proliferative effects on various cells, stimulation of hormone release and modulation of central nervous activity. During embryogenesis, the Edn1–Ednra axis regulates craniofacial and cardiovascular morphogenesis, whereas the Edn3–Ednrb axis contributes to melanocyte and enteric neuron development (Kurihara et al., 1999, 1994; Sato et al., 2008b).

The Edn system has been known to play pleiotropic roles in renal (patho)physiology. In the renal vasculature, Edn1 exerts potent vasoconstriction mainly through both Ednra (Hirata et al., 1989; Honing et al., 2000), whereas some vascular beds show an endothelium-dependent vasodilatory response mediated by Ednrb (Matsumura et al., 2000). Edn1 also acts on renal tubules to promote diuresis and natriuresis by several mechanisms via Ednrb (Ahn et al., 2004; Gariepy et al., 2000; Tomita et al., 1993). Furthermore, Edn1 modulates renin secretion from juxtaglomerular (JG) cells (Rakugi et al., 1988). Through these effects, the Edn system has been implicated in the pathophysiology of hypertension and various renal diseases.

To dissect mechanisms underlying these diverse roles of the Edn system, identification of cells expressing the Edn receptors is of fundamental importance. However, accurate description of their expression patterns remains still elusive due to relatively low expression levels and lack of antibodies sufficient for immunostaining. We have recently established mouse lines in which marker genes such as *lacZ* and *EGFP* are 'knocked-in' to the *Ednra* locus (Asai et al., 2010; Sato et al., 2008a). In these mice, the marker gene expression faithfully recapitulates that of the endogenous *Ednra* during embryogenesis. In this study, we analyzed these mice for renal expression to clarify the localization of Ednra and its developmental changes in the kidney.

1. Results

1.1. Isolation of Ednra–EGFP-positive cells and gene expression profiling by RT-PCR

In *Ednra-lacZ* or *-EGFP* knock-in mice, marker gene expression patterns faithfully recapitulate those of endogenous *Ednra*

* Corresponding author. Tel.: +81 3 5841 3498; fax: +81 3 5684 4958.
E-mail address: kuri-tky@umin.ac.jp (H. Kurihara).
[1] These authors contributed equally to this study.
[2] Present address: Yamanaka iPS Cell Special Project, Japan Science and Technology Agency, Kawaguchi 332-0012, Japan.

1567-133X/$ - see front matter © 2011 Elsevier B.V. All rights reserved.
doi:10.1016/j.gep.2011.04.001

expression in the heart and pharyngeal arches (Asai et al., 2010; Sato et al., 2008a). To confirm that *Ednra-lacZ/EGFP* expression also reflects endogenous *Ednra* expression in the kidney, we performed FACS and RT-PCR. Cells were isolated from the E17.5 *Ednra*$^{EGFP/+}$ kidneys and subjected to forward-side selection to preliminarily identify cells (Fig. 1A), FACS analysis using fluorescent lectin revealed that endothelial cells (detected by BS-1), proximal tubules (detected by LTA) and collecting ducts (detected by DBA) were sufficiently collected (Fig. S1), indicating that overall cell populations of the kidneys were properly obtained through our manipulation. After PI-selection to exclude non-viable cells (Fig. 1B), EGFP-positive and -negative cells were sorted for RT-PCR analysis (Fig. 1C). *Ednra*-expressing cells were detected only in the EGFP-positive fraction, while *Ednrb* expression was detectable only in the EGFP-negative fraction (Fig. 1D). This result indicates that the knocked-in EGFP expression appears to faithfully recapitulate endogenous *Ednra* expression and there is little overlapping in the expression of *Ednra* and *Ednrb* in the developing kidney. *Platelet-endothelial cell adhesion molecule-1* (*PECAM1/CD31*; a marker for endothelial cells) and *α-smooth muscle actin* (*αSMA*; a marker for smooth muscle cells) expression was detected only in the EGFP-negative and -positive fractions, respectively (Fig. 1D). This finding coincides with the distinct expression pattern of Edn receptors in vasculature: *Ednra* and *Ednrb* in smooth muscle cells and endothelial cells, respectively (Masaki, 2004).

RT-PCR also revealed that *aquaporin-1* (*Aqp1*; a marker for proximal renal tubules) and *aquaporin-3* (*Aqp3*; a marker for collecting ducts) expression was undetectable in the EGFP-positive fractions (Fig. 1D). Instead, *glial cell line-derived neurotrophic factor* (*GDNF*; a marker for undifferentiated mesenchyme) and *renin-1* (*Ren1*; a marker for juxtaglomerular cells) expression was found only in the EGFP-positive fractions (Fig. 1D). These results indicate that *Ednra*-expressing cell population is likely to include vascular smooth muscle cells, JG cells and undifferentiated mesenchymal cells.

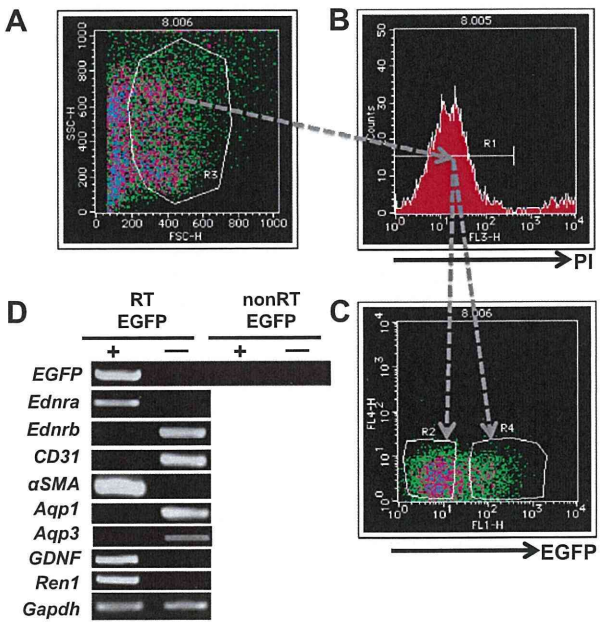

Fig. 1. Characterization of *Ednra-lacZ/EGFP*-expressing cells in the kidney. (A–C) Cells from the E17.5 *Ednra*$^{EGFP/+}$ embryonic kidneys were sorted into EGFP-positive and EGFP-negative fractions. Cells are subjected to forward-side selection for preliminary identification of the cells (A), next PI selection was performed to exclude nonviable cells (B), and finally EGFP selection was carried out to identify EGFP-expressing and EGFP-non-expressing cells (C). Gated R2 and R4 regions correspond to fractions of EGFP-negative and -positive cells, respectively. (D) RT-PCR analysis of EGFP-positive and -negative cells from the E17.5 kidneys. *Ednra* was detected only in the *Ednra–EGFP*-positive fraction. Expression of *Ednrb*, *CD31*, *αSMA*, *Aqp1*, *GDNF*, and *Ren1* was also analyzed. *Gapdh* was used as an internal control.

1.2. LacZ- and EGFP-labeling reveals the renal expression pattern of Ednra and its developmental changes

To analyze the expression pattern of *Ednra* in the kidney, we performed β-galactosidase staining on *Ednra-lacZ* knock-in embryonic and adult kidneys. *LacZ*-expressing cells were detected as early as E12.5 in mesenchyme around ureteric buds, although their expression levels were low compared to those in the lung and testis interstitium, where *Ednra* was most abundantly expressed at this stage (Fig. 2A and B). At E15.5 (Fig. 2C–E) and E18.5 (Fig. 2F–H), when basic expression patterns of *lacZ* are almost the same, *lacZ* expression was broadly distributed mainly in the medullary interstitial mesenchyme (Fig. 2C, D and F). By contrast, *lacZ* expression was relatively low in the cortical nephrogenic region (Fig. 2C, E and F). In higher magnification images, *lacZ*-expressing cells were detected in the vessel wall (Fig. 2G) and in the JG region encompassing intraglomerular mesangium and afferent and efferent arterioles (Fig. 2D–F). In adult sections, *lacZ* expression was apparently much sparser than in embryonic ones (compare Fig. 2I to C and F). At higher magnifications, *lacZ*-positive cells were observed around vessels (Fig. 2J) and in the JG region (Fig. 2K) as in embryonic sections. But, compared to developing kidneys, *lacZ*-positive cells were much decreased in the interstitium and inside the glomerulus. Throughout kidney development, renal tubular epithelium was not stained for β-galactosidase. These observations are consistent with the results of RT-PCR analysis described above.

To confirm that the *lacZ* expression patterns faithfully recapitulate the endogenous expression of *Ednra* in the kidney, we performed in situ hybridization on E18.5 kidney sections. *Ednra* expression was mainly distributed in the medullary interstitial region (Fig. S2A and B). High magnification images detected *Ednra* expression in the medullary interstitium (Fig. S2C and D), vessels (Fig. S2E) and the JG region (Fig. S2F). By contrast, renal tubules are apparently *LacZ*-negative (Fig. S2C–F). These patterns are largely identical to *Ednra-lacZ* expression patterns shown in Fig. 2.

To further dissect the characters of *Ednra*-expressing cells in the kidneys, we performed double immunostaining on *Ednra–EGFP* knock-in embryos and adult mice. We used CD31 and αSMA as markers for endothelial and smooth muscle cells, respectively. At E18.5, EGFP-expressing cells were detected around CD31-positive vascular endothelial cells and in the JG region (Fig. 3A–A‴). CD31-negative glomerular mesangial cells also showed EGFP expression (Fig. 3A–A‴). αSMA-positive cells are broadly observed along vessels and they are EGFP-positive (Fig. 3B–B‴). In the JG region, αSMA expression fades away as previously described (Sauter et al., 2008), and only EGFP signals remain (Fig. 3B–B‴). In addition, αSMA-negative and EGFP-positive cells were found in the interstitium (Fig. 3B–B‴).

In adult sections, EGFP signal was sparse, as seen in β-galactosidase staining. EGFP-expressing cells were detected in the vascular medial wall underlying CD31-positive endothelial cells (Fig. 3C–C‴) and in the JG region (Fig. 3D–D‴). Interestingly, EGFP expression in glomerular mesangial cells and the interstitium apparently was much less than in the developing kidney. To determine the character of *Ednra*-expressing cells in the interstitium, we observed some sections and checked approximately 1500 EGFP-positive cells, and found all the EGFP signals adjacent to CD31 signals (Fig. 3E–E‴), indicating that these *Ednra*-expressing cells are likely to be pericytes surrounding the descending vasa recta.

Taken these results together, *Ednra* expression in vascular smooth muscle cells and JG cells remain after birth, while